Rotation Invariant Vortices for Flow Visualization

Tobias Günther, Maik Schulze and Holger Theisel

Abstract— We propose a new class of vortex definitions for flows that are induced by rotating mechanical parts, such as stirring devices, helicopters, hydrocyclones, centrifugal pumps, or ventilators. Instead of a Galilean invariance, we enforce a rotation invariance, i.e., the invariance of a vortex under a uniform-speed rotation of the underlying coordinate system around a fixed axis. We provide a general approach to transform a Galilean invariant vortex concept to a rotation invariant one by simply adding a closed form matrix to the Jacobian. In particular, we present rotation invariant versions of the well-known Sujudi-Haimes, Lambda-2, and Q vortex criteria. We apply them to a number of artificial and real rotating flows, showing that for these cases rotation invariant vortices give better results than their Galilean invariant counterparts.

Index Terms—Vortex cores, rotation invariance, Galilean invariance, scientific visualization, flow visualization, line fields

1 Introduction

Vortices are among the most interesting structures in fluid flows, and frequently they are visually analyzed. Although there is a common understanding of what a vortex is, there is no unique definition featuring all desired properties. The definition of vortex concepts is an active field of research in a number of disciplines, such as mathematics, physics, and CFD. In recent years, the visualization community contributed new definitions of vortex concepts and efficient algorithms to their numerical computation. A common useful property of many vortex definitions is Galilean invariance, i.e., the invariance of the vortex under an equal-speed translation of the underlying coordinate system. In addition, there are a few approaches demanding the much stronger property of objectivity of a vortex, i.e., invariance under any smooth translation and rotation of the coordinate system.

This paper focuses on vortices in flows that are obtained by rotating mechanical parts around a fixed and known axis. Examples are stirring devices, helicopters, hydrocyclones, centrifugal pumps, or ventilators. To illustrate the problem, consider a cylindrical container filled with a fluid and an inserted propeller, as shown in Fig. 1(a). Rotating the propeller with constant angular speed induces a fluid motion. We are interested in its vortices. As depicted by a camera in Fig. 1(a), the observer has a fixed position above the container, meaning that the observer sees the propeller rotating and the container standing still. In Fig. 1(b), we have the same configuration, but now the observer is "sitting" on the propeller and rotating with it. This means that in the local coordinate system of the observer the propeller is standing still while the container is rotating. Computing vortices in the different reference frames usually gives different results, even though the applied vortex concepts are Galilean invariant. Which reference coordinate system should be used to get "correct" vortices? A first assumption may be that in areas close to the propeller configuration 1(b) gives better results because there the flow has a rotational speed similar to the propeller, and that close to the wall of the container configuration 1(a) is better if a no-slip boundary is assumed. This, however, raises the question how to treat the areas between propeller and wall. Because for those, the observer may have an optimal own rotation between zero and the propeller. In fact, the choice of the rotating reference frame of the observer has a great influence on the resulting vortices. How to choose it correctly?

- *Tobias Günther is with the Visual Computing Group at the University of Magdeburg. E-mail: tobias@isg.cs.ovgu.de.*
- *Maik Schulze is with MAXON Computer. E-mail: maik@isg.cs.ovgu.de.*
- *Holger Theisel is head of the Visual Computing Group at the University of Magdeburg. E-mail: theisel@ovgu.de.*

Manuscript received 31 Mar. 2015; accepted 1 Aug. 2015; date of publication xx xxx 2015; date of current version xx xxx 2015.
For information on obtaining reprints of this article, please send e-mail to: tvcg@computer.org.

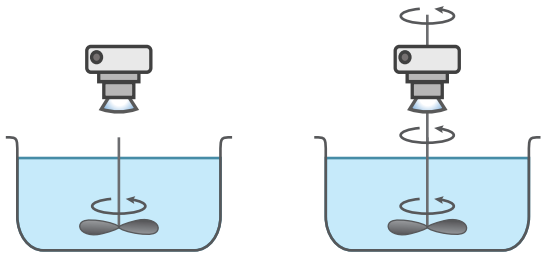

(a) Fixed reference frame (b) Rotating reference frame

Fig. 1. Rotating flow with different positions of the observer; (a) observer has a fixed position and sees the propeller rotate; (b) observer is "sitting" on the propeller and sees the propeller standing still.

This paper presents a solution for this problem: we propose new vortex concepts for which the choice of the rotating reference frame does not matter, i.e., vortex concepts that are invariant under the relative rotation of the observer. We call them *rotation invariant vortices*. Starting with a formal definition of rotation invariance, we present a simple and generic approach to transform a Galilean invariant vortex concept to a rotation invariant one. In fact, it reduces to a slight modification of the Jacobian, i.e., adding of a simple closed form matrix. We apply this to several standard vortex concepts: cores of swirling particle motion [43], λ_2 [16], and the Q criterion [15]. We demonstrate our method on several rotating flows, showing that the rotation invariant methods give better results than their Galilean invariant counterparts.

Notation

Given an n-dimensional ($n = 2,3$) time-dependent vector field $\mathbf{v}(\mathbf{x},t) = \mathbf{v}(x,y,[z,]t)$, we denote its partials as $\mathbf{v}_x, \mathbf{v}_y, [\mathbf{v}_z,]\mathbf{v}_t$, respectively. Interpreting the time-dependent field as an autonomous system in space-time, we can write it as an $(n+1)$-dimensional steady field $\overline{\mathbf{p}} = \begin{pmatrix}\mathbf{v}\\ 1\end{pmatrix}$. We provide the following measures in both n-D space and $(n+1)$-D space-time, where the latter is formally denoted by a bar.

Jacobian: The spatial Jacobian is $\mathbf{J} = \nabla\mathbf{v} = (\mathbf{v}_x, \mathbf{v}_y[, \mathbf{v}_z])$. The space-time Jacobian is $\overline{\mathbf{J}} = \nabla\overline{\mathbf{p}} = \begin{pmatrix}\mathbf{J} & \mathbf{v}_t\\ \mathbf{0}^{\mathrm{T}} & 0\end{pmatrix}$. We denote $\mathbf{e}_1, \mathbf{e}_2[, \mathbf{e}_3]$ the eigenvectors of $\mathbf{J}$. For $n = 3$ and the case that two eigenvalues are complex, the eigenvector to the only real eigenvalue is $\mathbf{e}$.

Acceleration: The acceleration in space is $\mathbf{a} = \mathbf{J}\mathbf{v} + \mathbf{v}_t$, the acceleration is space-time is $\overline{\mathbf{a}} = \overline{\mathbf{J}}\,\overline{\mathbf{p}}$. Note that $\overline{\mathbf{a}} = (\mathbf{a}, 0)^{\mathrm{T}}$.

Feature Flow Field: The feature flow field was originally introduced to track critical points in space-time [41]. Here, we will use

it for general vortex tracking. We define it in space-time as $\bar{\mathbf{f}}$ and in space as $\mathbf{f}$ by division by its last component. For $n = 2$ we have [41]

$$\bar{\mathbf{f}} = \begin{pmatrix} \det(\mathbf{v}_y, \mathbf{v}_t) \\ \det(\mathbf{v}_t, \mathbf{v}_x) \\ \det(\mathbf{v}_x, \mathbf{v}_y) \end{pmatrix}, \quad \mathbf{f} = \frac{1}{\det(\mathbf{v}_x, \mathbf{v}_y)} \begin{pmatrix} \det(\mathbf{v}_y, \mathbf{v}_t) \\ \det(\mathbf{v}_t, \mathbf{v}_x) \end{pmatrix}.$$

For $n = 3$ we have [43]

$$\bar{\mathbf{f}} = \begin{pmatrix} -\det(\mathbf{v}_y, \mathbf{v}_z, \mathbf{v}_t) \\ \det(\mathbf{v}_z, \mathbf{v}_t, \mathbf{v}_x) \\ -\det(\mathbf{v}_t, \mathbf{v}_x, \mathbf{v}_y) \\ \det(\mathbf{v}_x, \mathbf{v}_y, \mathbf{v}_z) \end{pmatrix}, \quad \mathbf{f} = \frac{1}{\det(\mathbf{v}_x, \mathbf{v}_y, \mathbf{v}_z)} \begin{pmatrix} -\det(\mathbf{v}_y, \mathbf{v}_z, \mathbf{v}_t) \\ \det(\mathbf{v}_z, \mathbf{v}_t, \mathbf{v}_x) \\ -\det(\mathbf{v}_t, \mathbf{v}_x, \mathbf{v}_y) \end{pmatrix}.$$

Note that $\mathbf{f}$ can only be computed if $\mathbf{J}$ is non-singular. Excluding parts with singular $\mathbf{J}$ from the computation is not a strong restriction because $\det(\mathbf{J}) = 0$ usually occurs on 2-manifolds in 3D only. Also note that $\bar{\mathbf{J}}$ has the eigenvectors $\begin{pmatrix} \mathbf{e}_1 \\ 0 \end{pmatrix}$, $\begin{pmatrix} \mathbf{e}_2 \\ 0 \end{pmatrix}$, $\left[\begin{pmatrix} \mathbf{e}_3 \\ 0 \end{pmatrix},\right] \bar{\mathbf{f}}$, where $\bar{\mathbf{f}}$ has the corresponding eigenvalue 0. There is a simple relation

$$\mathbf{v} - \mathbf{f} = \mathbf{J}^{-1}\,\mathbf{a} \tag{1}$$

that follows directly from the definitions of $\mathbf{J}$, $\mathbf{a}$ and $\mathbf{f}$, respectively, but has, to the best of our knowledge, not been mentioned in the literature.

Further, we denote the **Parallel Vectors Operator** [28] of two 3D vectors as $\parallel$, and the **Coplanar Vectors Operator** [43] of three 4D vectors as copl. If necessary, we make use of the ∇ operator. $\mathbf{I}$ denotes the identity matrix.

2 Related Work

Vortices are among the most important features in fluid flows and for this reason much research was devoted to their quantification, extraction and tracking. As there is no universal definition that captures all desired properties, a number of different vortex measures have been proposed in the literature [14, 15, 16, 31]. Overall, they can be categorized into region-based methods and line-based methods.

In region-based methods, volumes of vortex-like behavior are extracted, for instance by thresholding pressure, vorticity or helicity. In the CFD community, region-based measures such as the Q criterion by Hunt [15] and the λ_2-criterion by Jeong and Hussain [16] are well-established. Biswas et al. [5] combined four local region-based vortex detectors via majority voting, namely λ_2, Q, Δ [6] and Γ_2 [12]. Okubo [26] and Weiss [46] independently developed a criterion related to Q and more recently Haller [14] derived the objective $\mathbf{M}_z$ criterion. A region-based method finding nested vortices was developed by Petz et al. [29]. Kasten et al. [22] extracted Galilean invariant vortex regions by use of acceleration. Further, Kasten et al. [21] tracked vortex merging events over time by use of combinatorial scalar field topology. Combinatorial topology was also of concern in the vortex core region detection of Jiang et al. [18].

Line-based methods, on the other hand, search for lines that particles rotate around. For this, Banks and Singer [1] suggested a curve following velocity-predictor, pressure-corrector method. Sahner et al. [34] extracted extremum lines of region-based methods, naming the λ_2 criterion and Q criterion by the use of feature flow fields [41]. Later, Sahner et al. [35] computed vortex and strain skeletons as extremal structures of derived scalar quantities. Schafhitzel et al. [36] set further focus on the topology of λ_2-based vortex corelines.

For a 3D steady flow $\mathbf{v}$, Sujudi and Haimes [39] defined the reduced vorticity criterion, which considers the eigenvalues and eigenvectors of the Jacobian $\mathbf{J}$. A vortex coreline is present if a pair of complex-conjugate eigenvalues exists (necessary condition for swirling) and the eigenvector $\mathbf{e}$ to the remaining real eigenvalue fulfills: $\mathbf{v} - (\mathbf{v}^{\mathrm{T}}\mathbf{e})\mathbf{e} = \mathbf{0}$. This method extracts the coreline of swirling streamlines in 3D flow and has found many applications [10]. Peikert and Roth [28] formally defined the parallel vectors (PV) operator, which returns the set of points at which two vector fields are parallel. Using the PV operator Sujudi-Haimes is equivalently expressed as $\mathbf{v} \parallel \mathbf{J}\,\mathbf{v}$, i.e., $\mathbf{v}$ is parallel to an eigenvector of $\mathbf{J}$. A higher-order method was described later by Roth and Peikert [31] to extract bent vortex corelines.

Aside from physically-based vortex definitions, geometric methods can be found in the literature [27], which are useful for handling weak vortices. With the curvature centre method and the winding-angle method, Sadarjoen and Post [32] presented two geometric approaches that are based on streamline geometry. Köhler et al. [23] presented a semi-automatic method based on line predicates to assess vortices in cardiac blood flow. For unsteady data, Bauer and Peikert [2], and Theisel et al. [40] tracked the cores of swirling streamlines over time. This makes sense for vortex tracking in instantaneous vector fields, such as magnetic fields. Fuchs et al. [8] and Weinkauf et al. [43] found that pathlines swirl around a different coreline than streamlines and thus extended the method of Sujudi and Haimes in different ways to find cores of swirling pathlines, i.e., the cores of particles in unsteady flow. For this, Weinkauf et al. [43] derived a coplanar vectors condition that reduces to a parallel vectors operation.

Aside from the geometric methods, all aforementioned automatic extraction approaches have in common that they are local, and thus easily parallelizable. However, it was shown that there are classes of vortices that cannot be extracted by local methods, for instance attracting vortices that move on non-linear paths. Thus, instead, integration-based methods were developed, such as particle density estimation by Wiebel et al. [48]. They proposed to inject a number of particles and observe their attraction behavior over time. Weinkauf and Theisel [44] found attractors by analyzing the Jacobian of a derived vector field in which streaklines are tangent curves.

Another Lagrangian detector was developed by Cucitore et al. [7]. They extracted vortices by observing the neighboring particles around a particle to test, i.e., they let the reference frame move with the tested particle. Further, Lagrangian smoothing as proposed by Fuchs et al. [9] and Shi et al. [37] can be applied to any local vortex detector that was originally designed for steady flow by smoothing the extraction results along pathlines over time.

Orthogonal to vortex definitions are the verification of numerical extraction results and their further processing for visualization. Jiang et al. [17] presented a method to verify corelines based on the geometry of streamlines. To improve the vortex core visualization, Garth et al. [11] computed hull surfaces around vortex cores based on the Rankine vortex model. Sahner et al. [34] proposed an iconic representation to indicate scale and extent. For a more detailed overview on vortex extraction and visualization methods we refer to [25, 28, 30].

Aside from the definition of extraction methods that are invariant under certain types of reference frame motion (Galilean invariance, objectivity, rotation invariance), there is a thread of research on finding a suitable reference frame in which the flow appears (nearly) steady. A very common example is the subtraction of a mean flow (or a certain percentage of it that is based on domain expert experience), which is obsolete for Galilean invariant extraction methods [43]. More sophisticated reference frame choices use decompositions of the flow to find a harmonic vector field that can be subtracted to eliminate the general motion. Since harmonic fields are divergence-free and curl-free, the resulting field keeps its local divergence and rotation properties. Wiebel et al. [49] decomposed the flow into a localized and a harmonic component, and studied the localized component, with the restriction that the localized flow is confined into a domain. The Helmholtz-Hodge decomposition (HHD) [3] decomposes a vector field into a scalar potential (curl-free), a vector potential (divergence-free) and a harmonic vector field. If the latter is present, the resulting components and the uniqueness of the decomposition strongly depend on the boundary conditions. Bathia et al. [4] used their *natural* HHD to extract vortices in the resulting (near-)steady flow. Aside from using the HHD to perform a change of the reference frame, vortices have also been characterized as extremal structures of the magnitude of the vector potential, e.g., by Tong et al. [42] and Wiebel et al. [47].

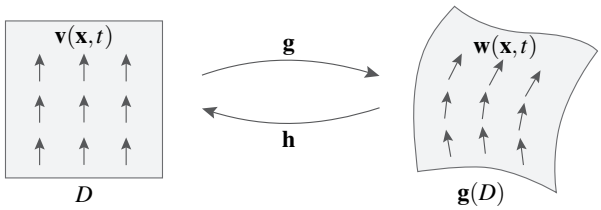

Fig. 2. Creating a new vector field $\mathbf{w}$ by a domain transformation $\mathbf{g}$.

3 Domain deformation, Galilean invariance and objectivity

Much of the argumentation in this paper will be based on the concept of *domain deformation*. In fact, we use it for two purposes: to formally define the concept of Galilean invariance, objectivity and rotation invariance, and to find practical computations of rotation invariant vortex measures.

3.1 Domain deformation

Given the vector field $\mathbf{v}(\mathbf{x},t)$ in the spatial domain D and the temporal domain T, we consider a domain deformation as a differentiable map

$$\mathbf{g} : D \times T \to D \tag{2}$$

which is a diffeomorphism in its reduction to any $t \in T$. This means that there is a unique inverse map $\mathbf{h} : D \times T \to D$ with

$$\mathbf{h}(\mathbf{g}(\mathbf{x},t),t) = \mathbf{g}(\mathbf{h}(\mathbf{x},t),t) = \mathbf{x} \tag{3}$$

for any $(\mathbf{x},t) \in D \times T$. Based on $\mathbf{g}$, we define a new vector field in the domain $\mathbf{g}(D)$ that transforms pathlines: for every pathline $(\mathbf{q}(t),t)$ in $\mathbf{v}$, the transformed line $(\mathbf{g}(\mathbf{q}(t),t),t)$ is a pathline in $\mathbf{w}$. This property uniquely defines $\mathbf{w}$ as [24]

$$\mathbf{w}(\mathbf{x},t) = (\nabla \mathbf{h}(\mathbf{x},t))^{-1} (\mathbf{v}(\mathbf{h}(\mathbf{x},t),t) - \mathbf{h}_t(\mathbf{x},t)) \tag{4}$$

where $\nabla \mathbf{h}$ is the spatial gradient of $\mathbf{h}$ and $\mathbf{h}_t$ is its derivative with respect to time. We call $\mathbf{w}$ the *domain transformed vector field* inducted by the domain transformation $\mathbf{g}$. Figure 2 illustrates this. Eq. (4) can be inverted to transform $\mathbf{w}$ back to $\mathbf{v}$:

$$\mathbf{v}(\mathbf{x},t) = (\nabla \mathbf{g}(\mathbf{x},t))^{-1} (\mathbf{w}(\mathbf{g}(\mathbf{x},t),t) - \mathbf{g}_t(\mathbf{x},t)) \tag{5}$$

3.2 Galilean invariance

A vortex measure is *Galilean invariant* if it is invariant under an equal-speed translation of the underlying coordinate system. By using the concept of domain deformation we can formalize this by

Definition 1 *A vortex measure is Galilean invariant if for any transformation*

$$\mathbf{g}(\mathbf{x},t) = \mathbf{x} + \mathbf{c}_0 + t\,\mathbf{c} \tag{6}$$

where $\mathbf{c}_0$ is a constant point and $\mathbf{c}$ is a constant vector, the following holds: the vortex measure classifies a point $(\mathbf{x},t)$ to be on the vortex in $\mathbf{v}$ iff the vortex measure classifies the point $(\mathbf{g}(\mathbf{x},t),t)$ to be on a vortex in the domain transformed field $\mathbf{w}$.

Common local Galilean invariant measures are $\mathbf{J}$ and $\mathbf{a}$. Any measure that contains only $\mathbf{J},\mathbf{a}$, their derivatives or a Lagrangian aggregation of them over time is Galilean invariant as well. Examples are cores of swirling particle motion [43], λ_2, Okubo-Weiss, FTLE and FSLE. For $n = 2$ we also have the following Galilean invariant conditions that are all equivalent in areas of non-vanishing Jacobian:

$$\mathbf{a} = \mathbf{0} \quad \Leftrightarrow \quad \mathbf{v} - \mathbf{f} = \mathbf{0} \quad \Leftrightarrow \quad \bar{\mathbf{f}} \parallel \bar{\mathbf{p}} \quad \Leftrightarrow \quad \bar{\mathbf{J}}\,\bar{\mathbf{p}} \parallel \bar{\mathbf{p}}. \tag{7}$$

The equivalence of the four expressions in (7) follows directly from Eq. (1), $\bar{\mathbf{J}}\,\bar{\mathbf{p}} = (\mathbf{a},0)^{\mathrm{T}}$ and $\bar{\mathbf{p}} = (\mathbf{v},1)^{\mathrm{T}}$. As a side note, it means that for $n = 2$ the cores of swirling particle motion [43] and vortices by vanishing acceleration [22, 20] are identical. For $n = 3$ there are the following equivalent conditions for a non-singular Jacobian [43]:

$$\mathrm{copl}\left(\bar{\mathbf{p}},\bar{\mathbf{f}},\begin{pmatrix}\mathbf{e}\\0\end{pmatrix}\right) \quad \Leftrightarrow \quad \mathbf{e} \parallel \mathbf{v} - \mathbf{f} \quad \Leftrightarrow \quad \mathbf{J}(\mathbf{v} - \mathbf{f}) \parallel \mathbf{v} - \mathbf{f}, \tag{8}$$

all of them giving Galilean invariant vortices.

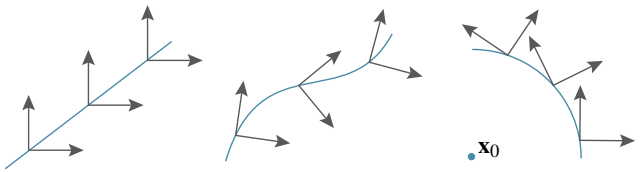

(a) Galilean invariance (b) Objectivity (c) Rotation invariance

Fig. 3. Invariance under different transformations of the coordinate frame (i.e., the camera): Galilean invariant (left), objective (middle), rotation invariant (right).

3.3 Objectivity

A vortex measure is *objective* if it is invariant under any smooth translation and rotation of the reference system. The formal definition has the same form as Definition 1, except that (6) is replaced by

$$\mathbf{g}(\mathbf{x},t) = \mathbf{Q}(t)\,\mathbf{x} + \mathbf{c}(t) \tag{9}$$

where $\mathbf{Q}(t)$ is a time-dependent rotation matrix and $\mathbf{c}(t)$ is a time-dependent translation vector. The strain tensor $\mathbf{S} = \frac{1}{2}(\mathbf{J} + \mathbf{J}^{\mathrm{T}})$ is known to be objective. Any Lagrangian aggregation of it or its derivatives is objective as well, as done in the $\mathbf{M}_z$ criterion in [14]. Figure 3 illustrates the concepts.

4 Rotation invariance

To give a formal definition of rotation invariance, we consider a fixed rotation center point $\mathbf{x}_0 = (x_0,y_0)^{\mathrm{T}}$ for $n = 2$ or a fixed rotation axis given by a point $\mathbf{x}_0$ and a normalized vector $\mathbf{n}$ for $n = 3$. Then, the definition of rotation invariance has the same form as Definition 1 when replacing (6) for $n = 2$ by

$$\mathbf{g}(\mathbf{x},t) = \begin{pmatrix}\cos(\omega\,t+\omega_0) & \sin(\omega\,t+\omega_0)\\ -\sin(\omega\,t+\omega_0) & \cos(\omega\,t+\omega_0)\end{pmatrix}(\mathbf{x}-\mathbf{x}_0) + \mathbf{x}_0 \tag{10}$$

and for $n = 3$ by

$$\mathbf{g}(\mathbf{x},t) = \mathbf{Q}_0^{-1}\begin{pmatrix}\cos(\omega\,t+\omega_0) & \sin(\omega\,t+\omega_0) & 0\\ -\sin(\omega\,t+\omega_0) & \cos(\omega\,t+\omega_0) & 0\\ 0 & 0 & 1\end{pmatrix}\mathbf{Q}_0\,(\mathbf{x}-\mathbf{x}_0) + \mathbf{x}_0 \tag{11}$$

where $\mathbf{Q}_0$ is the rotation matrix transforming $\mathbf{n}$ to the z-axis and ω,ω_0 are arbitrary scalars. Note that (10) and (11) describe rotations with constant angular speed of the observer around a fixed point/axis. Also note that up to now all introduced domain transformations (6), (9), (10) and (11) describe isometric deformations, i.e., they transform a square to a square of the same size.

Clearly, standard Galilean invariant vortex concepts like cores of swirling particle motion, λ_2, or Q are generally not rotation invariant. We describe now a simple generic approach to transform a Galilean invariant concept to a rotation invariant one. For $n = 2$, we introduce a non-isometric domain deformation $\mathbf{g}_p(\mathbf{x},t)$ and its inverse $\mathbf{h}_p(\mathbf{x},t)$

$$\mathbf{g}_p(\mathbf{x},t) = \begin{pmatrix}\arctan\frac{y-y_0}{x-x_0}\\ \|\mathbf{x}-\mathbf{x}_0\|\end{pmatrix}, \quad \mathbf{h}_p(\mathbf{x},t) = \mathbf{x}_0 + y\begin{pmatrix}\cos x\\ \sin x\end{pmatrix} \tag{12}$$

along with its domain transformed vector field $\mathbf{w}_p$. Eq. (12) describes a domain transformation to polar coordinates. Instead of applying a Galilean invariant vortex criterion to $\mathbf{v}$ at $(\mathbf{x},t)$, we apply it to $\mathbf{w}_p$ at $\mathbf{g}_p(\mathbf{x},t)$. In other words: we domain transform $\mathbf{v}$ to polar coordinates, do the vortex extraction there, and transform the resulting vortex structures back to the original Cartesian coordinates. Note that this gives in general different vortex structures than an application of the vortex measure in Cartesian coordinates because the non-isometric domain transformation induces a non-linear transformation of the Jacobian. Also note that this way we obtain a rotation invariant vortex measure if the vortex measure applied to $\mathbf{w}_p$ is Galilean invariant: an equal-speed rotation around $\mathbf{x}_0$ in the domain of $\mathbf{v}$ corresponds to an equal-speed

translation of the coordinate system in the domain of $\mathbf{w}_p$. Hence, a Galilean invariant measure in $\mathbf{w}_p$ becomes a rotation invariant measure in $\mathbf{v}$.

Although the domain transformation to polar coordinates is the theoretical solution of our problem, it creates new practical problems concerning the computation of the Jacobian in polar coordinates. In particular, it is unclear on which discretization to compute the Jacobian in polar coordinates since the domain transformation $\mathbf{g}_p$ maps cells with planar faces in Cartesian coordinates to cells of different size and density with non-planar faces in polar coordinates. To address this problem, we present an approach to compute the (modified) Jacobian in Cartesian coordinates only, without a transformation to polar coordinates. For this, we can directly use the grid discretization coming from the simulation. To introduce this, we keep in mind that most vortex measures are computed by a certain combination of $\mathbf{v}$, $\mathbf{v}_t$ and $\mathbf{J}$. This means that after the domain transformation we have to consider $\mathbf{w}_p(\mathbf{g}_p(\mathbf{x},t),t)$ and its Jacobian $\mathbf{J}_p(\mathbf{g}_p(\mathbf{x},t),t) = \nabla(\mathbf{w}_p(\mathbf{g}_p(\mathbf{x},t),t))$. Instead of considering $\mathbf{w}_p$ and $\mathbf{J}_p$, we transform them back to Cartesian coordinates

$$\mathbf{v}_r(\mathbf{x},t) = (\nabla \mathbf{g}_p(\mathbf{x},t))^{-1} \cdot \mathbf{w}_p(\mathbf{g}_p(\mathbf{x},t),t) \tag{13}$$

$$\mathbf{v}_{rt}(\mathbf{x},t) = (\nabla \mathbf{g}_p(\mathbf{x},t))^{-1} \cdot \frac{\partial}{\partial t}\mathbf{w}_p(\mathbf{g}_p(\mathbf{x},t),t) \tag{14}$$

$$\mathbf{J}_r(\mathbf{x},t) = (\nabla \mathbf{g}_p(\mathbf{x},t))^{-1} \cdot \nabla(\mathbf{w}_p(\mathbf{g}_p(\mathbf{x},t),t)). \tag{15}$$

Fortunately, (13)–(15) have a simple closed form:

$$\mathbf{v}_r = \mathbf{v} \tag{16}$$

$$\mathbf{v}_{rt} = \frac{\partial \mathbf{v}_r}{\partial t} = \mathbf{v}_t \tag{17}$$

$$\mathbf{J}_r = \mathbf{J} + \frac{1}{d}\,\mathbf{R}\,\mathbf{H}\,\mathbf{R}^{\mathrm{T}} = (\mathbf{v}_{xr}, \mathbf{v}_{y_r}) \tag{18}$$

with

$$d = \|\mathbf{x}-\mathbf{x}_0\| \quad , \quad \mathbf{r} = \frac{\mathbf{x}-\mathbf{x}_0}{d} \quad , \quad \mathbf{r}_p = \begin{pmatrix} 0 & 1 \\ -1 & 0 \end{pmatrix} \mathbf{r} \tag{19}$$

and the 2D matrices

$$\mathbf{R} = (\mathbf{r}_p, \mathbf{r}) \quad , \quad \mathbf{H} = \begin{pmatrix} -\mathbf{v}^{\mathrm{T}}\mathbf{r} & -\mathbf{v}^{\mathrm{T}}\mathbf{r}_p \\ \mathbf{v}^{\mathrm{T}}\mathbf{r}_p & 0 \end{pmatrix}. \tag{20}$$

See the appendix for a derivation. Eqs. (16)–(18) have an interesting meaning: in order to transform a Galilean invariant vortex measure to a rotation invariant one, we only have to replace $\mathbf{J}$ by $\mathbf{J}_r$. Note that $\mathbf{J}_r$ is obtained by adding a closed-form matrix to $\mathbf{J}$, meaning that we do not have to worry about grid discretization in a transformation.

From the rotation invariant Jacobian, we directly get rotation invariant acceleration and feature flow field:

$$\mathbf{a}_r = \mathbf{J}_r\,\mathbf{v} + \mathbf{v}_t \;\; , \;\; \bar{\mathbf{a}}_r = \bar{\mathbf{J}}_r\,\bar{\mathbf{p}} \tag{21}$$

with

$$\bar{\mathbf{J}}_r = \begin{pmatrix} \mathbf{J}_r & \mathbf{v}_t \\ \mathbf{0}^{\mathrm{T}} & 0 \end{pmatrix}, \tag{22}$$

and

$$\bar{\mathbf{f}}_r = \begin{pmatrix} \det(\mathbf{v}_{y_r}, \mathbf{v}_t) \\ \det(\mathbf{v}_t, \mathbf{v}_{xr}) \\ \det(\mathbf{v}_{xr}, \mathbf{v}_{y_r}) \end{pmatrix} \;, \; \mathbf{f}_r = \frac{1}{\det(\mathbf{v}_{xr}, \mathbf{v}_{y_r})} \begin{pmatrix} \det(\mathbf{v}_{y_r}, \mathbf{v}_t) \\ \det(\mathbf{v}_t, \mathbf{v}_{xr}) \end{pmatrix}.$$

The case $n = 3$ is similar and a straightforward extension of the case $n = 2$. Instead of a domain deformation to polar coordinates, we do a deformation to cylindrical coordinates around the axis given by $\mathbf{x}_0, \mathbf{n}$. A transformation of the Jacobian back to Cartesian space gives the rotation invariant Jacobian

$$\mathbf{J}_r = \mathbf{J} + \frac{1}{d}\,\mathbf{R}\,\mathbf{H}\,\mathbf{R}^{\mathrm{T}} = (\mathbf{v}_{xr}, \mathbf{v}_{y_r}, \mathbf{v}_{zr})$$

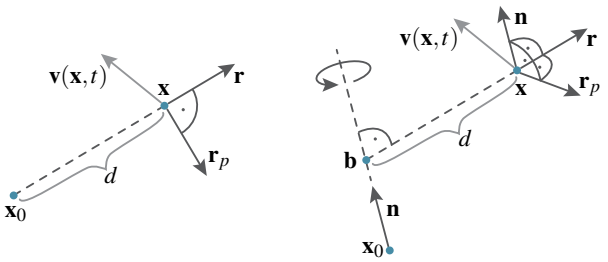

Fig. 4. Setup for computing the rotation invariant Jacobian for $n = 2$ (left) and $n = 3$ (right).

with $\mathbf{b}$ being the point on the rotation axis with shortest distance to $\mathbf{x}$, i.e., $(\mathbf{x}-\mathbf{b})^{\mathrm{T}}\mathbf{n} = 0$, and

$$d = \|\mathbf{x}-\mathbf{b}\| \quad , \quad \mathbf{r} = \frac{\mathbf{x}-\mathbf{b}}{d} \quad , \quad \mathbf{r}_p = \mathbf{r}\times\mathbf{n} \tag{23}$$

and the 3D matrices

$$\mathbf{R} = (\mathbf{r}_p, \mathbf{r}, \mathbf{n}) \quad , \quad \mathbf{H} = \begin{pmatrix} -\mathbf{v}^{\mathrm{T}}\mathbf{r} & -\mathbf{v}^{\mathrm{T}}\mathbf{r}_p & 0 \\ \mathbf{v}^{\mathrm{T}}\mathbf{r}_p & 0 & 0 \\ 0 & 0 & 0 \end{pmatrix}. \tag{24}$$

This gives for rotation invariant acceleration the same forms (21)–(22) as for $n = 2$, and for the rotation invariant feature flow field we have

$$\bar{\mathbf{f}}_r = \begin{pmatrix} -\det(\mathbf{v}_{y_r}, \mathbf{v}_{z_r}, \mathbf{v}_t) \\ \det(\mathbf{v}_{z_r}, \mathbf{v}_t, \mathbf{v}_{xr}) \\ -\det(\mathbf{v}_t, \mathbf{v}_{xr}, \mathbf{v}_{y_r}) \\ \det(\mathbf{v}_{xr}, \mathbf{v}_{y_r}, \mathbf{v}_{z_r}) \end{pmatrix}, \; \mathbf{f}_r = \frac{1}{\det(\mathbf{v}_{xr}, \mathbf{v}_{y_r}, \mathbf{v}_{z_r})} \begin{pmatrix} -\det(\mathbf{v}_{y_r}, \mathbf{v}_{z_r}, \mathbf{v}_t) \\ \det(\mathbf{v}_{z_r}, \mathbf{v}_t, \mathbf{v}_{xr}) \\ -\det(\mathbf{v}_t, \mathbf{v}_{xr}, \mathbf{v}_{y_r}) \end{pmatrix}.$$

Figure 4 illustrates the setups for 2D and 3D.

5 Rotation Invariant Vortex Measures

We can now propose particular rotation invariant vortex measures by inserting $\mathbf{J}_r$ in their respective definitions.

5.1 Rotation invariant cores of swirling particle motion

For $n = 2$, any condition of (7) gives Galilean invariant cores of swirling particle motion. For rotation invariant cores of swirling particle motion we propose any of the following equivalent conditions:

$$\mathbf{a}_r = \mathbf{0} \quad \Leftrightarrow \quad \mathbf{v}-\mathbf{f}_r = \mathbf{0} \quad \Leftrightarrow \quad \bar{\mathbf{f}}_r \parallel \bar{\mathbf{p}} \quad \Leftrightarrow \quad \bar{\mathbf{J}}_r\,\bar{\mathbf{p}} \parallel \bar{\mathbf{p}}. \tag{25}$$

For $n = 3$, the Galilean invariant conditions are in (8). In addition to this, we propose a new Galilean invariant vortex measure:

$$\nabla(\mathbf{v}-\mathbf{f})\cdot(\mathbf{v}-\mathbf{f}) \parallel (\mathbf{v}-\mathbf{f}), \tag{26}$$

i.e., we apply Sujudi-Haimes to $\mathbf{v}-\mathbf{f}$. In case of vortices moving along an equal-speed translation, we can assume $\nabla\mathbf{f} = \mathbf{0}$, meaning that (8) and (26) show the same vortices. However, in the rotation invariant case, (26) performs better, as shown later in Section 6.4. We propose

$$\nabla(\mathbf{v}-\mathbf{f}_r)\cdot(\mathbf{v}-\mathbf{f}_r) \parallel (\mathbf{v}-\mathbf{f}_r) \tag{27}$$

for rotation invariant cores of swirling particle motion.

5.2 Rotation invariant region-based methods

For the definition of rotation invariant region-based measures, we consider the decomposition of the rotation invariant Jacobian

$$\mathbf{J}_r = \mathbf{S}_r + \Omega_r \tag{28}$$

into the rate-of-strain tensor $\mathbf{S}_r = \frac{1}{2}(\mathbf{J}_r + \mathbf{J}_r^{\mathrm{T}})$ and the vorticity tensor $\Omega_r = \frac{1}{2}(\mathbf{J}_r - \mathbf{J}_r^{\mathrm{T}})$. Following [16], we define the rotation invariant λ_{2r} criterion by considering the second-largest eigenvalue of $\mathbf{S}_r^2 + \Omega_r^2$:

$$\lambda_{2r} = \lambda_2(\mathbf{S}_r^2 + \Omega_r^2) < 0. \tag{29}$$

Similarly, we follow [15] and define the rotation invariant Q_r criterion

$$Q_r = \frac{1}{2}\left(\|\Omega_r\|^2 - \|\mathbf{S}_r\|^2\right) > 0, \tag{30}$$

which characterizes vortices as regions in which the Euclidean norm of the rotation invariant vorticity tensor dominates that of the rotation invariant rate-of-strain tensor.

6 Results

In the following, we demonstrate the rotation invariant vortex measures. We use several synthetic data sets and study two real-world flows.

6.1 Beads

The Beads flow was reported by Wiebel et al. [48] and has previously been among the most challenging benchmarks for vortex extraction. An analytic approximation to it was given in [44]:

$$\mathbf{v}(x,y,t) = \begin{pmatrix} -(y - \frac{1}{3}\sin(t)) - (x - \frac{1}{3}\cos(t)) \\ (x - \frac{1}{3}\cos(t)) - (y - \frac{1}{3}\sin(t)) \end{pmatrix}. \tag{31}$$

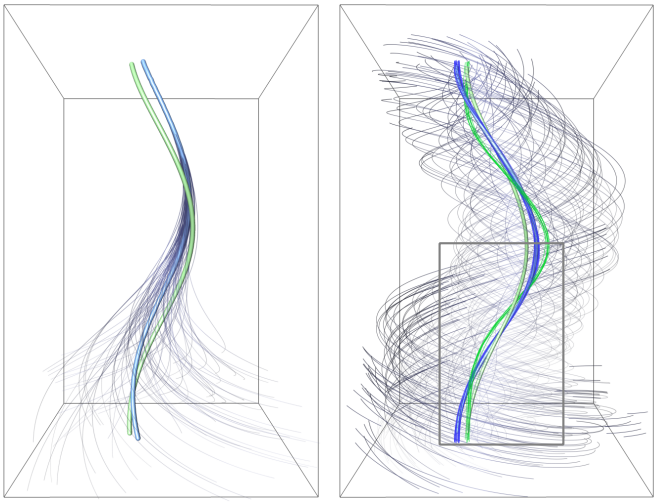

(a) Standard Beads flow. (b) Divergence-free Beads flow.

(c) Galilean invariant coreline with pathlines. (d) Rotation invariant coreline with pathlines. (e) Images (c) and (d) shown together.

Fig. 5. Local coreline extraction in the standard Beads flow in (a), and its divergence-free version in (b), both visualized in space-time where time denotes the vertical axis. Images (c)–(e) show close-ups of (b), with the pathline seeds being depicted by colored spheres. Green corelines are obtained by the Galilean invariant cores of swirling particle motion (wrong result), whereas blue corelines are computed with our rotation invariant extension (correct result). In image (b)–(e), pathlines are seeded on the extracted corelines, showing that green pathlines (seeded at Galilean invariant coreline) spiral away, whereas blue pathlines stay at the rotation invariant coreline.

The flow is defined in the domain $D \times T = [-2,2]^2 \times [0, 2\pi]$. Previously, all local vortex extractors failed and only integration-based methods could find the solution [44, 13], such as particle density estimation [48, 13] or cores of swirling streaklines [44]. As shown in Fig. 5(a), our rotation invariant method is the first local method that finds the correct coreline, which was identified by Weinkauf et al. [44] as the pathline $\mathbf{x}(t) = \frac{1}{3}(\sin(t) + \cos(t), -\cos(t) + \sin(t))^{\mathrm{T}}$.

We go a step further and consider a modification of the Beads flow that cannot be handled by integration-based particle density estimation, as it is *divergence-free*. Thus, neither standard local nor integration-based methods are applicable. That is, a center moving on a circle:

$$\mathbf{v}(x,y,t) = \begin{pmatrix} -2y + \frac{2}{3}\sin(t) \\ 2x - \frac{2}{3}\cos(t) \end{pmatrix}, \tag{32}$$

again defined in the domain $D \times T = [-2,2]^2 \times [0, 2\pi]$. Fig. 5(b) depicts the rotation invariant coreline and swirling pathlines as context, showing that our method delivers correct results in this data set, too. Here, the correct coreline is the pathline $\mathbf{x}(t) = \frac{2}{3}(\cos(t), \sin(t))^{\mathrm{T}}$.

6.2 Four Rotating 2D Centers

The Four Centers (SC) data set is based on the scalar field

$$s(x,y) = 3xy \cdot e^{-x^2-y^2} \tag{33}$$

and is defined in the domain $D = [-2, 2]^2$. Its co-gradient vector field contains four centers. The abbreviation SC stems from *streamline core*, as we construct the unsteady flow by rotation of the streamlines, which prescribes the location of the streamline cores. That is, over time, we slice-by-slice rotate the underlying scalar field around $\mathbf{x}_0 = \mathbf{0}$, considering it in the temporal domain $T = [0, 2\pi]$:

$$\mathbf{v}(x,y,t) = \begin{pmatrix} \frac{\partial}{\partial y} s(x',y') \\ -\frac{\partial}{\partial x} s(x',y') \end{pmatrix} \tag{34}$$

with $\begin{pmatrix} x' \\ y' \end{pmatrix} = \begin{pmatrix} \cos(t) & \sin(t) \\ -\sin(t) & \cos(t) \end{pmatrix} \begin{pmatrix} x \\ y \end{pmatrix}$. Equivalently, the flow can be constructed by adding a center with the angular velocity of the above rotation, and transforming the flow using Eqs. (5) and (10) from the rotating reference frame into the fixed reference frame. While the steady field contains four streamline vortex corelines, the rotating system exhibits only two pathline cores, as shown in Fig. 6. This cancellation of cores is due to the addition of the center in the analogous flow in the rotating reference frame. We use this flow to demonstrate the rotation invariance of our method in Fig. 7. A direct application of Galilean invariant pathline cores [43] (which are for 2D unsteady flows identical to Sujudi-Haimes [39] in space-time), as in Fig. 7(a) does not find the correct rotation centers, as shown by green pathlines leaving

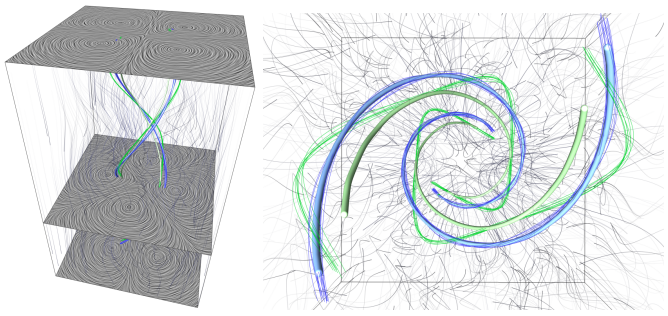

Fig. 6. Space-time visualization of the 2D unsteady Four centers (SC) flow, with the camera viewing along the time axis and gray pathlines as context. Green corelines are obtained by cores of swirling motion, the blue corelines are their rotation invariant counterparts. As visible by the green and blue pathlines, only rotation invariant cores exhibit swirling motion in their vicinity.

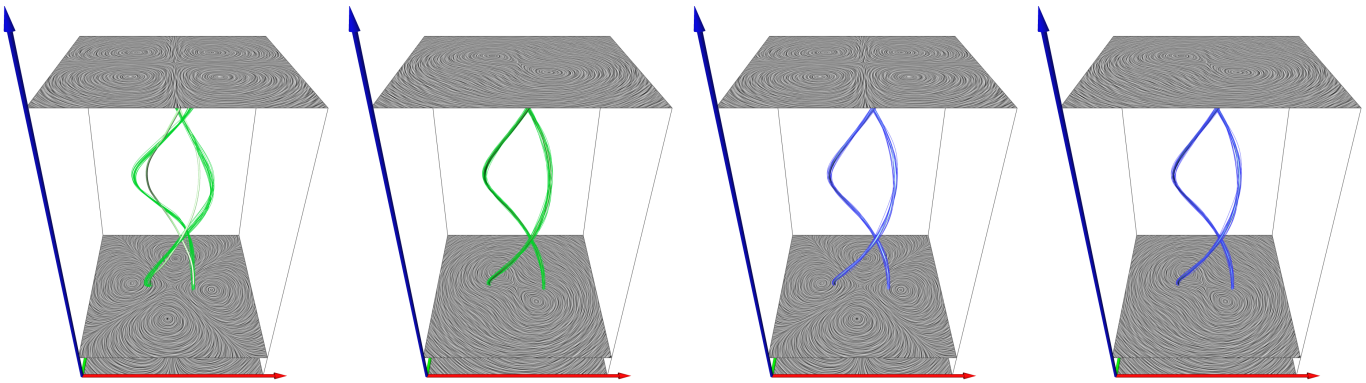

(a) Galilean invariant pathline cores (original reference frame) (b) Galilean invariant pathline cores (modified reference frame) (c) Rotation invariant pathline cores (original reference frame) (d) Rotation invariant pathline cores (modified reference frame)

Fig. 7. The 2D unsteady FOUR CENTERS (SC) flow in space-time. Direct application of (Galilean invariant) pathline cores [43] in (a) does not reveal the correct corelines. It does produce correct corelines after an appropriate change of the reference frame (b). Our rotation invariant pathline cores in (c) and (d) find the centers of swirling motion in rotating systems regardless of the reference frame.

the coreline. In this data set, a prior change to an appropriate reference frame, as in Fig. 7(b), removes the rotational movement, making Galilean invariant pathline cores applicable. In this paper, we extend existing Galilean invariant vortex core extractors to become *rotation invariant*, which extracts the correct rotation centers, regardless of the reference frame, see Figs. 7(c) and 7(d).

Next, we construct another unsteady vector field named FOUR CENTERS (PC) by prescribing the flow in the rotating frame as:

$$\mathbf{w}(\hat{x},\hat{y},t) = \begin{pmatrix} -\hat{x}\cdot e^{-\hat{x}^2-\hat{y}^2}(2\hat{y}^2-1) \\ \hat{y}\cdot e^{-\hat{x}^2-\hat{y}^2}(2\hat{x}^2-1) \end{pmatrix} \tag{35}$$

with coordinates in the rotating frame $(\hat{x},\hat{y})^{\mathrm{T}} = \mathbf{g}(\mathbf{x},t)$ and rotate it using Eqs. (5) and (10) with $\omega = 1$ and $\omega_0 = 0$ into the fixed frame.

With this, we prescribe the rotation of *pathline cores* (PC). In the fixed frame, the centers vanish, as visible in Fig. 8 (left). This time, we find four rotation invariant pathline cores, but only two (wrong) cores with the Galilean invariant counterpart. Our rotation invariant coreline extraction finds the correct cores of swirling pathlines in both unsteady flows (SC) and (PC).

Next, we compare the Galilean invariant region-based vortex criteria λ_2 and Q with their rotation invariant versions λ_{2r} and Q_r in the flow with prescribed pathline cores (PC), i.e., we know that there are four vortices to expect. Fig. 9 (left) shows an overview of the methods, containing Galilean invariant pathline cores (green), rotation invariant pathline cores (blue), Galilean invariant region-based methods (red) and rotation invariant region-based methods (yellow). The top right image shows the Galilean invariant techniques, which detect only two cores. The green pathlines spiral away from the vortex corelines, showing that the classic Galilean invariant method delivers incorrect results. The bottom right image shows our rotation invariant extensions, which extract four vortex cores, as expected. The blue pathlines show that the rotation invariant vortex coreline is indeed the correct coreline.

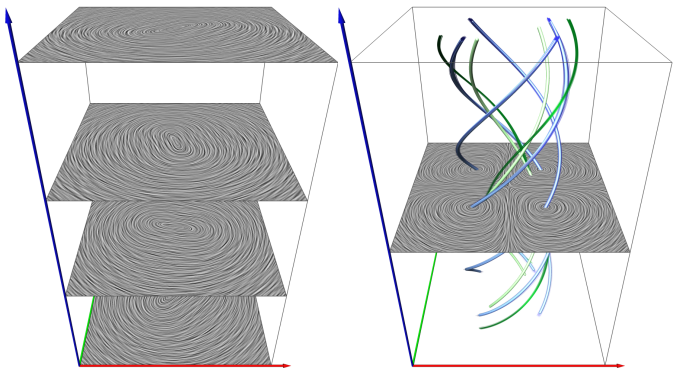

Fig. 8. FOUR CENTERS (PC) flow with prescribed centers in the rotating reference frame in space-time. In the fixed reference frame (left), the four centers partly vanished. Corelines were extracted in the fixed reference frame. The right image shows a LIC slice of the rotating frame, displaying the four centers.

6.3 Two Spiraling 2D Centers

A major strength of rotation invariance is that the angular speed of the underlying rotation must not be known in advance to obtain accurate extraction results. This is very helpful for non-linear rotations, in which the underlying rotation is unknown or difficult to describe. An example is a system in which the angular speed decays or increases with distance to the center of rotation. We built a synthetic test data set to demonstrate such situation. We place centers at $(1,0)^{\mathrm{T}}$ and $(2,0)^{\mathrm{T}}$ in the rotating reference frame:

$$\mathbf{w}(\hat{x},\hat{y},t) = \begin{pmatrix} -2\hat{y} \\ 4\hat{x}^3 - 18\hat{x}^2 + 26\hat{x} - 12 \end{pmatrix} \tag{36}$$

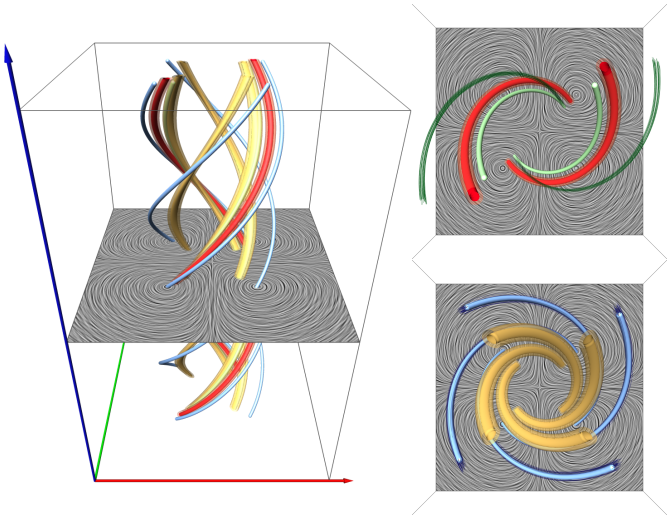

Fig. 9. Region-based methods in the FOUR CENTERS flow in space-time. Left: Overview image. Top right: Galilean invariant methods (two cores). Bottom right: Rotation invariant methods (four cores). Opaque isosurfaces show λ_2 (top) and λ_{2r} (bottom) and transparent isosurfaces depict Q (top) and Q_r (bottom). Here, Q and λ_2 deliver similar results. The same applies for Q_r and λ_{2r}.

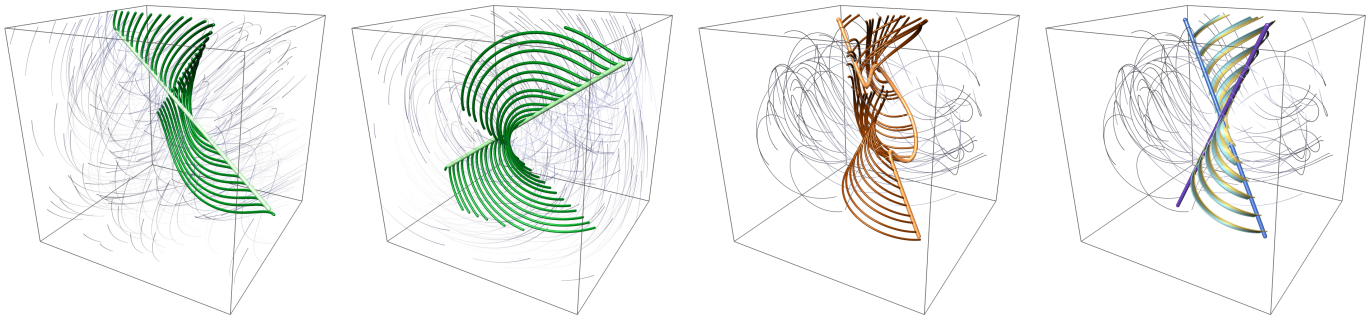

(a) Streamline core by Sujudi-Haimes at $t = 1$, streamlines in background.

(b) Streamline core by Sujudi-Haimes at $t = 4$, streamlines in background.

(c) A direct extension of [43], i.e., $\mathbf{J}_r(\mathbf{v}-\mathbf{f}_r) \parallel (\mathbf{v}-\mathbf{f}_r)$ is incorrect.

(d) Our correct rotation invariant pathline cores at $t = 1$ and $t = 4$.

Fig. 11. Vortex cores in the ROTATING CENTER flow, with pathlines starting or ending at the corelines. Figs. (a) and (b) depict the flow at two instantaneous time steps, with streamlines in the background. A direct extension of cores of swirling particle motion yields wrong results (c). Image (d) shows the rotation invariant pathline cores at $t = 1$ (dark blue) and $t = 4$ (dark purple). Pathline ribbons from $t = 1...4$ connect the two corelines, showing both the coreline's movement path and the rotational movement of particles by the ribbon twist.

with coordinates in the rotating frame $(\hat{x},\hat{y})^{\mathrm{T}} = \mathbf{g}(\mathbf{x},t)$ and transform it using Eqs. (5) and (10) with $\omega = 0.3(x^2+y^2)$ and $\omega_0 = 0$ into the fixed reference frame. We consider the flow in the domain $D \times T = [-2.5, 2.5]^2 \times [-\pi,\pi]$, as shown in Fig. 10. Note that in this flow the distance of a particle to the center of rotation remains constant, and thus a particle's angular speed does not change. It can be seen that with lower angular speed (closer to the global rotation center) the difference to cores of swirling particle motion becomes smaller, as the vector field is more steady, i.e., the temporal derivative $\frac{\mathrm{d}\mathbf{v}}{\mathrm{d}t}$ is smaller. As shown by the pathlines, our rotation invariant method accurately extracts the vortex cores of swirling pathlines.

6.4 Rotating 3D Center

In the following, we construct a time-dependent 3D vector field. At time $t = 0$, it contains a center with its coreline through the points $(1,0,0)^{\mathrm{T}}$ and $(0,1,1)^{\mathrm{T}}$. (At $t = 0$, this coreline can be found using Sujudi-Haimes.) Over time, we rotate the center globally slice-by-slice around the z-axis, i.e., $\mathbf{x}_0 = \mathbf{0}$ and $\mathbf{n} = (0,0,1)^{\mathrm{T}}$. The resulting field in a fixed reference frame is defined in the domain $D \times T = [-5,5]^3 \times [0,2\pi]$ as:

$$\mathbf{v}(x,y,z,t) = \begin{pmatrix} \frac{\sqrt{3}}{3}(z\cos(t)+z\sin(t)-\cos(t)-y) \\ \frac{\sqrt{3}}{3}(z\cos(t)-z\sin(t)+\sin(t)+x) \\ -\frac{\sqrt{3}}{3}(x\cos(t)+y\cos(t)+x\sin(t)-y\sin(t)-2) \end{pmatrix}$$

Fig. 11 depicts the rotating center and the vortex corelines therein. In Fig. 11(a) a streamline core is shown for $t = 1$ with pathlines seeded at the coreline and integrated up to $t = 4$. Similarly, Fig. 11(b) contains the streamline core of $t = 4$, with backwards integrated pathlines to $t = 1$. Comparing both, we see that pathlines seeded from one coreline do not reach the other coreline. Thus, the traced particles have not been seeded at a true vortex core. A direct extension of cores of swirling particle motion [43] does not result in the correct corelines, as shown in Fig. 11(c). With our proposed generalization (27), the rotation invariant pathline cores can be found. This is demonstrated by the pathline ribbons that were seeded on one coreline and have reached the other. Further, their twist shows the swirling behavior of nearby particles. Note that this vector field has no Galilean invariant pathline cores, since $\det(\mathbf{J}) = 0$.

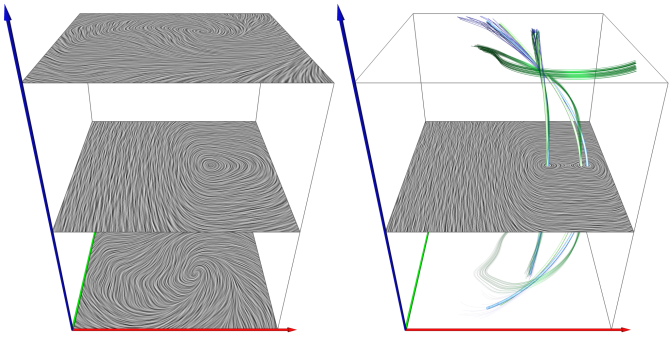

Fig. 10. TWO SPIRALING CENTERS in space-time with their center positions prescribed in the rotating reference frame. The left image visualizes the fixed reference frame, which was used to extract the corelines shown on the right. In the right image, pathlines were released from the corelines, and a LIC slice of the rotating reference frame is shown, displaying the two centers.

6.5 Centrifugal Pump

Our first real-world data set was subject of the IEEE Visualization Contest 2011. The data is courtesy of the Institute of Applied Mechanics, Clausthal University, Germany and was made available by Dipl. Wirtsch.-Ing. Andreas Lucius. We consider an unsteady 2D slice ($z = 0.01$) of the simulated flow based on the DES turbulence model, which is already provided in a rotating reference frame. Common practice is to track vortices in a reference frame rotating with the angular velocity of the blades. As we will show, this rotating frame is not ideal as the vortices are moving in the blank areas between the blades. In fact, our rotation invariant extractor finds cores of better quality. Fig. 12(a) depicts cores of swirling particle motion and our rotation invariant pathline cores.

In the following, we explain how we evaluate the quality of the extracted corelines. Unfortunately, there is no ground truth location, since there is no universal vortex measure that can be considered best. There is, however, a rather commonly desired coreline property: Corelines should ideally be pathlines, since they would then represent particles that other particles swirl around, and hence, we get cores of swirling particle motion. We measure this property by the tangent alignment with the flow. We define the *tangent alignment* $\tau_{\mathbf{c}}(t)$ of a coreline $\mathbf{c}(t)$ as a scalar line attribute that is defined as the absolute value of the dot product between (space-time) vector field $\overline{\mathbf{p}}$ and the tangent of the space-time coreline $\overline{\mathbf{c}}(t) = \begin{pmatrix} \mathbf{c}(t) \\ t \end{pmatrix}$ (both normalized):

$$\tau_{\mathbf{c}}(t) = \left| \frac{\overline{\mathbf{p}}(\overline{\mathbf{c}}(t),t)}{\|\overline{\mathbf{p}}(\overline{\mathbf{c}}(t),t)\|} \cdot \frac{\mathrm{d}\overline{\mathbf{c}}(t)/\mathrm{d}t}{\|\mathrm{d}\overline{\mathbf{c}}(t)/\mathrm{d}t\|} \right| . \tag{37}$$

As visible in Fig. 12(b), Galilean invariant cores of swirling particle motion have a poorer tangent alignment than our rotation invariant pathline cores, shown in Fig. 12(c).

6.6 Rotating Mixer

Our second real-world data set features a rotating mixer, which was provided by Gábor Janiga, who is with the Institute of Fluid Dynam-

(a) Galilean (green) and rotation invar. (blue) cores. (b) Galilean invariant - Tangent alignment (c) Rotation invariant - Tangent alignment

(d) Galilean (green) and rotation invar. (blue) cores. (e) Galilean invariant - Tangent alignment (f) Rotation invariant - Tangent alignment

Fig. 12. Vortex cores of a CENTRIFUGAL PUMP in a rotating reference frame in space-time. While Galilean and rotation invariant vortex cores are similar (a), the Galilean invariant cores (b) have a poorer tangent alignment than our rotation invariant counterpart (c). The bottom row (d)-(f) shows a close-up of the region highlighted in (a).

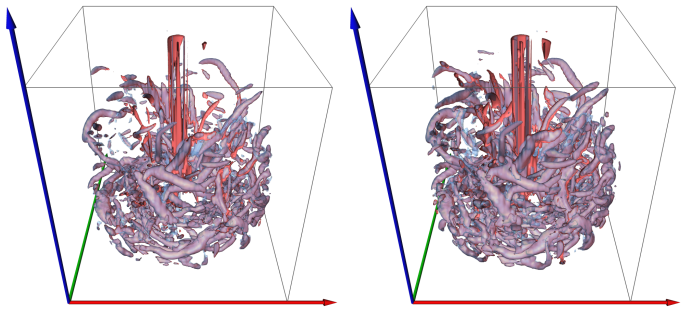

(a) isosurfaces $\lambda_2 = -60$ and $\lambda_{2r} = -60$ (b) isosurfaces $Q = 40$ and $Q_r = 40$

Fig. 13. Region-based techniques in the ROTATING MIXER data set. Backfaces of the red isosurfaces depict the standard Galilean invariant λ_2 and Q criteria. The frontfaces of blue isosurfaces show our rotation invariant counterparts λ_{2r} and Q_r.

ics and Thermodynamics, University of Magdeburg, Germany. This vector field is given in a fixed reference frame. Fig. 13 displays isosurfaces of the λ_2, Q, λ_{2r} and Q_r criteria, for the time step $t = 0.004$. The left image shows Galilean invariant (red) and rotation invariant (blue) isosurfaces for $\lambda_2 = -60$ and $\lambda_{2r} = -60$, respectively. With the Q criterion we examined very similar results for $Q = 60$ and $Q_r = 60$. The right image depicts Galilean invariant (red) and rotation invariant (blue) isosurfaces for $Q = 40$ and $Q_r = 40$. Similarly, $\lambda_2 = -40$ and $\lambda_{2r} = -40$ give similar results. For such turbulent real-world flows a ground truth is unknown, and thus it is hard to quantify which vortex extraction method works better. We observed that Galilean invariant and rotation invariant surfaces differed only slightly in their strength (isovalue). We found the largest differences in the proximity of the mixer geometry. Apparently, those areas are more influenced by rotating motion. The cylindrical mixer geometry itself becomes apparent too, but is largely a boundary artifact.

7 IMPLEMENTATION AND EVALUATION

7.1 Coreline Extraction and Filtering

As shown earlier, our rotation invariant corelines are expressed by the parallel vectors operator. Peikert and Roth [28] explained several methods for PV extraction, which can be applied here. For all examples shown in the paper, we used the parallel vectors implementation of the visualization toolkit Amira [38]. The computation involves the setup of the vector fields to test for parallelism and a prior test for presence of complex eigenvalues in the rotation invariant Jacobian $\mathbf{J}_r$, which is a necessary swirling condition. After extraction, a tangent alignment filter using Eq. (37) is applied to remove lines that are not tangential enough to the flow, followed by subsequent joining of close line segments to fill gaps and a final thresholding of lines by length to remove the remaining noise. All these filter steps are considered as standard procedure in local coreline extraction methods. There are a number of alternatives for closed PV line extraction including the curve-following predictor-corrector method of Peikert and Roth [28] or the use of stable feature flow fields as in Weinkauf et al. [45]. For cell-based extractions, Ju et al. [19] recently proposed a robust parity test to determine the number of PV points per cell face.

7.2 Performance

Our modifications to enable rotation invariance are only local and rapidly computed. They are much faster compared to the actual parallel vectors extraction in the line-based techniques and the computation of eigenvalues in the region-based techniques. Thus, the performance is very similar to standard Galilean invariant techniques. Space-time grid sizes and extraction times are shown in Table 1 for our rotation invariant pathline cores. The timings are measured on a system with an Intel Core i7-2600K CPU with 3.4 GHz and 24 GB RAM. The computation time linearly depends on the number of voxels with complex-conjugate eigenvalues in the Jacobian. For instance, in the FOUR CENTERS (SC) flow more voxels could be skipped than in the BEADS flows, due to the prior test for swirling behavior. Timings for the region-based techniques are shown in Table 2. As the Q_r

Data set	Grid size	Extraction time
BEADS (STD)	$64 \times 64 \times 64$	20.7 sec.
BEADS (DIV.-FREE)	$64 \times 64 \times 64$	20.9 sec.
FOUR CENTERS (SC)	$64 \times 64 \times 64$	4.5 sec.
FOUR CENTERS (PC)	$128 \times 128 \times 128$	55.2 sec.
SPIRALING CENTERS	$128 \times 128 \times 128$	55.6 sec.
ROTATING CENTER	$64 \times 64 \times 64$	20.2 sec.
CENTRIFUGAL PUMP	$512 \times 512 \times 80$	7.5 min.

Table 1. Total computation time of rotation invariant pathline cores.

criterion comes almost for free with the computation of λ_{2r} because $Q_r = -\frac{1}{2}(\lambda_{1r} + \lambda_{2r} + \lambda_{3r})$, we list combined timings, i.e., the time required to compute the eigenvalues and from those λ_{2r} and Q_r.

8 Discussion and Limitations

Simplicity: Our technique to compute rotation invariant vortices is extremely simple: just add a closed form matrix to the Jacobian and feed the vortex extractor with it. There is virtually no computation overhead or performance and accuracy drop in comparison to the original methods.

Relation to objective vortices: Clearly, an objective vortex is also rotation invariant: objectivity is a much stronger property than rotation invariance. However, existing objective vortex measures can be "too strong" to find expected vortices in a standard data set. An example can be found in [33], where the $\mathbf{M}_z$ criterion of [14] is applied to a cylinder flow: the objective $\mathbf{M}_z$ does not detect the typical von Kármán vortex street behind the cylinder. In particular, we are not aware of an objective measure that detects the correct vortex in the divergence-free BEADS data set.

Restriction to rotating flows: Our technique makes only sense for flows that are induced by a rotating movement around an axis. We think that this class of flows is large enough to make our approach relevant. Note that moving the rotation center/axis to infinity lets $\mathbf{J}_r$ converge to $\mathbf{J}$ and therefore converges to a Galilean invariant technique. Another issue is that for our technique one must know the location of the rotation point/axis. We do not consider this as a strong restriction because this information usually comes with the data set.

No Galilean invariance: We stress again that our technique is not Galilean invariant anymore. We argue that, for the data considered here, rotation invariance is more important than Galilean invariance. The better vortex structures shown in this paper confirm this assumption.

9 Conclusions

In this paper, we made the following contributions:

- We identified rotation invariance as desirable property for vortex measures in flows that are induced by rotating parts.
- We gave a formal definition of rotation invariance.
- We have shown an extremely simple way to transform a Galilean invariant measure to a rotation invariant one: we simply have to add a closed form matrix to the Jacobian and feed the vortex extractor with it.
- We proposed rotation invariant versions of cores of swirling particle motion, λ_2 and Q.
- We have applied them to a number of data sets, showing that our technique gives better vortices than the Galilean invariant measures. In particular, our technique is – to the best of our knowledge – the first local method that finds the exact core in the standard and divergence-free BEADS flow.

In addition to this, the paper contains some minor contributions:

Data set	Grid size	Extraction time
ROTATING MIXER	$256 \times 256 \times 128$	36.5 sec.
FOUR CENTERS (PC)	$256 \times 256 \times 256$	2.3 min.

Table 2. Total computation time of rotation invariant λ_{2r} and Q_r.

- We have formulated a simple relation between $\mathbf{v}$, $\mathbf{J}$, $\mathbf{a}$ and $\mathbf{f}$ that holds both for $n = 2$ and $n = 3$, namely Eq. (1).
- We have shown that for $n = 2$, acceleration-based techniques [22, 20] and cores of swirling particle motion [43] give the same corelines for non-singular $\mathbf{J}$.
- For $n = 3$, we proposed a slight variation of the cores of swirling particle motion [43] in (26). In fact, this paper proposes to apply Sujudi-Haimes on $\mathbf{v} - \mathbf{f}$. While this does not affect the results in the Galilean invariant case, it improves the results for the rotation invariant case.

Acknowledgments

This work was partially supported by the DFG grant TH 692/8-1.

Appendix

In the following, we briefly show how Eqs. (16)–(18) are derived from Eqs. (13)–(15). First, Eq. (16) follows from (13) and

$$\mathbf{w}_p(\mathbf{g}_p(\mathbf{x},t),t) = (\nabla \mathbf{h}_p(\mathbf{g}_p(\mathbf{x},t),t))^{-1} \cdot \mathbf{v}(\mathbf{h}_p(\mathbf{g}_p(\mathbf{x},t),t),t) \quad (38)$$

which follows from (4). Applying the chain rule to the identity $\mathbf{h}_p(\mathbf{g}_p(\mathbf{x},t),t) = \mathbf{x}$, we get

$$\nabla(\mathbf{h}_p(\mathbf{g}_p(\mathbf{x},t),t)) = \nabla \mathbf{h}_p(\mathbf{g}_p(\mathbf{x},t),t) \cdot \nabla \mathbf{g}_p((\mathbf{x},t),t) = \nabla \mathbf{x} = \mathbf{I} \quad (39)$$

from which we get

$$(\nabla \mathbf{h}_p(\mathbf{g}_p(\mathbf{x},t),t))^{-1} = \nabla \mathbf{g}_p((\mathbf{x},t),t) \quad (40)$$

This and (13) give (16). Eq. (17) follows from the fact that $\mathbf{g}_p$ and $\mathbf{h}_p$ do not depend on t. To show (18), we apply the chain rule to (15):

$$\mathbf{J}_r(\mathbf{x},t) = (\nabla \mathbf{g}_p(\mathbf{x},t))^{-1} \cdot \nabla \mathbf{w}_p(\mathbf{g}_p(\mathbf{x},t),t) \cdot \nabla \mathbf{g}_p(\mathbf{x},t) \quad (41)$$

and insert

$$\nabla \mathbf{g}_p(\mathbf{x},t) = \begin{pmatrix} \frac{-(y-y_0)}{\|\mathbf{x}-\mathbf{x}_0\|^2} & \frac{(x-x_0)}{\|\mathbf{x}-\mathbf{x}_0\|^2} \\ \frac{(x-x_0)}{\|\mathbf{x}-\mathbf{x}_0\|} & \frac{(y-y_0)}{\|\mathbf{x}-\mathbf{x}_0\|} \end{pmatrix} \quad (42)$$

which follows from (12). See the additional material for an extended Maple proof.

References

[1] D. C. Banks and B. A. Singer. A predictor-corrector technique for visualizing unsteady flow. *IEEE Transactions on Visualization and Computer Graphics*, 1:151–163, 1995.

[2] D. Bauer and R. Peikert. Vortex tracking in scale-space. In *Proc. Symposium on Data Visualisation*, pages 233–240, 2002.

[3] H. Bhatia, G. Norgard, V. Pascucci, and P.-T. Bremer. The Helmholtz-Hodge decomposition–A survey. *IEEE Transactions on Visualization and Computer Graphics*, 19(8):1386–1404, 2013.

[4] H. Bhatia, V. Pascucci, R. M. Kirby, and P.-T. Bremer. Extracting features from time-dependent vector fields using internal reference frames. *Computer Graphics Forum (Proc. EuroVis)*, 33(3):21–30, 2014.

[5] A. Biswas, W. He, Q. Deng, C.-M. Chen, H.-W. Shen, R. Machiraju, and A. Rangarajan. An uncertainty-driven approach to vortex analysis using oracle consensus and spatial proximity. In *Proc. IEEE Pacific Visualization Symposium*, Hangzhou, China, 2015.

[6] M. S. Chong, A. E. Perry, and B. J. Cantwell. A general classification of threedimensional flow fields. *Physics of Fluids A: Fluid Dynamics*, 2(5):765–777, 1990.

[7] R. Cucitore, M. Quadrio, and A. Baron. On the effectiveness and limitations of local criteria for the identification of a vortex. *European Journal of Mechanics - B/Fluids*, 18(2):261–282, 1999.

[8] R. Fuchs, R. Peikert, H. Hauser, F. Sadlo, and P. Muigg. Parallel vectors criteria for unsteady flow vortices. *IEEE Transactions on Visualization and Computer Graphics*, 14(3):615–626, 2008.

[9] R. Fuchs, R. Peikert, F. Sadlo, B. Alsallakh, and M. E. Gröller. Delocalized unsteady vortex region detectors. In *Proc. Vision, Modeling and Visualization*, pages 81–90, 2008.

[10] C. Garth, R. S. Laramee, X. Tricoche, J. Schneider, and H. Hagen. Extraction and visualization of swirl and tumble motion from engine simulation data. In *Topology-based Methods in Visualization*, Visualization and Mathematics, pages 121–135. Springer Berlin Heidelberg, 2007.

[11] C. Garth, X. Tricoche, T. Salzbrunn, T. Bobach, and G. Scheuermann. Surface techniques for vortex visualization. In *Proc. Joint Eurographics - IEEE TCVG Conference on Visualization*, VISSYM'04, pages 155–164. Eurographics Association, 2004.

[12] L. Graftieaux, M. Michard, and N. Grosjean. Combining PIV, POD and vortex identification algorithms for the study of unsteady turbulent swirling flows. *Measurement Science and Technology*, 12(9):1422, 2001.

[13] T. Günther and H. Theisel. Vortex cores of inertial particles. *IEEE Transactions on Visualization and Computer Graphics (Proc. IEEE Scientific Visualization)*, 20(12):2535–2544, 2014.

[14] G. Haller. An objective definition of a vortex. *Journal of Fluid Mechanics*, 525:1–26, 2005.

[15] J. C. R. Hunt. Vorticity and vortex dynamics in complex turbulent flows. *Transactions on Canadian Society for Mechanical Engineering (Proc. CANCAM)*, 11(1):21–35, 1987.

[16] J. Jeong and F. Hussain. On the identification of a vortex. *Journal of Fluid Mechanics*, 285:69–94, 1995.

[17] M. Jiang, R. Machiraju, and D. Thompson. Geometric verification of swirling features in flow fields. In *Proc. IEEE Visualization*, pages 307–314, 2002.

[18] M. Jiang, R. Machiraju, and D. Thompson. A novel approach to vortex core region detection. In *Proc. Symposium on Data Visualisation (VISSYM)*, pages 217–226, 2002.

[19] T. Ju, M. Cheng, X. Wang, and Y. Duan. A robust parity test for extracting parallel vectors in 3D. *IEEE Transactions on Visualization and Computer Graphics (Proc. IEEE SciVis)*, 20(12):2526–2534, 2014.

[20] J. Kasten, I. Hotz, B. R. Noack, and H.-C. Hege. On the extraction of long-living features in unsteady fluid flows. In *Topological Methods in Data Analysis and Visualization*, Mathematics and Visualization, pages 115 – 126. Springer Berlin Heidelberg, 2011.

[21] J. Kasten, I. Hotz, B. R. Noack, and H.-C. Hege. Vortex merge graphs in two-dimensional unsteady flow fields. In *EuroVis - Short Papers*, pages 1–5, 2012.

[22] J. Kasten, J. Reininghaus, I. Hotz, and H.-C. Hege. Two-dimensional time-dependent vortex regions based on the acceleration magnitude. *IEEE Transactions on Visualization and Computer Graphics (Proc. IEEE SciVis)*, 17(12):2080–2087, 2011.

[23] B. Köhler, R. Gasteiger, U. Preim, H. Theisel, M. Gutberlet, and B. Preim. Semi-automatic vortex extraction in 4D PC-MRI cardiac blood flow data using line predicates. *IEEE Transactions on Visualization and Computer Graphics (Proc. IEEE Scientific Visualization)*, 19(12):2773–2782, 2013.

[24] A. Kuhn, C. Rössl, T. Weinkauf, and H. Theisel. A benchmark for evaluating FTLE computations. In *Proc. IEEE Pacific Visualization Symposium*, pages 121–128, Seoul, South-Korea, March 2012.

[25] R. S. Laramee, H. Hauser, L. Zhao, and F. H. Post. Topology-based flow visualization, the state of the art. In *Topology-based Methods in Visualization*, Mathematics and Visualization, pages 1–19. Springer Berlin Heidelberg, 2007.

[26] A. Okubo. Horizontal dispersion of floatable particles in the vicinity of velocity singularities such as convergences. *Deep Sea Research and Oceanographic Abstracts*, 17(3):445–454, 1970.

[27] H.-G. Pagendarm, B. Henne, and M. Rutten. Detecting vortical phenomena in vector data by medium-scale correlation. In *Proc. Visualization '99*, pages 409–552, 1999.

[28] R. Peikert and M. Roth. The "parallel vectors" operator – a vector field visualization primitive. In *Proc. IEEE Visualization*, pages 263–270, 1999.

[29] C. Petz, J. Kasten, S. Prohaska, and H.-C. Hege. Hierarchical vortex regions in swirling flow. *Computer Graphics Forum (Proc. EuroVis)*, 28(3):863–870, 2009.

[30] F. H. Post, B. Vrolijk, H. Hauser, R. S. Laramee, and H. Doleisch. The state of the art in flow visualisation: Feature extraction and tracking. *Computer Graphics Forum*, 22(4):775–792, 2003.

[31] M. Roth and R. Peikert. A higher-order method for finding vortex core lines. In *Proc. IEEE Visualization*, pages 143–150, 1998.

[32] I. A. Sadarjoen and F. H. Post. Geometric methods for vortex extraction. In *Data Visualization 99*, Eurographics, pages 53–62. Springer Vienna, 1999.

[33] J. Sahner. *Extraction of Vortex Structures in 3D Flow Fields*. PhD thesis, University of Magdeburg, Germany, April 2009.

[34] J. Sahner, T. Weinkauf, and H.-C. Hege. Galilean invariant extraction and iconic representation of vortex core lines. In *Proc. Eurographics / IEEE VGTC Symposium on Visualization (EuroVis)*, pages 151–160, 2005.

[35] J. Sahner, T. Weinkauf, N. Teuber, and H.-C. Hege. Vortex and strain skeletons in Eulerian and Lagrangian frames. *IEEE Transactions on Visualization and Computer Graphics*, 13(5):980–990, 2007.

[36] T. Schafhitzel, J. Vollrath, J. Gois, D. Weiskopf, A. Castelo, and T. Ertl. Topology-preserving lambda2-based vortex core line detection for flow visualization. *Computer Graphics Forum (Proc. EuroVis)*, 27(3):1023–1030, 2008.

[37] K. Shi, H. Theisel, H. Hauser, T. Weinkauf, K. Matkovic, H.-C. Hege, and H.-P. Seidel. Path line attributes - an information visualization approach to analyzing the dynamic behavior of 3D time-dependent flow fields. In *Topology-Based Methods in Visualization II*, Mathematics and Visualization, pages 75–88. Springer, 2009.

[38] D. Stalling, M. Westerhoff, and H.-C. Hege. Amira: A highly interactive system for visual data analysis. In *The Visualization Handbook*, pages 749–767. Elsevier, 2005.

[39] D. Sujudi and R. Haimes. Identification of swirling flow in 3D vector fields. Technical report, Departement of Aeronautics and Astronautics, MIT, 1995. AIAA Paper 95-1715.

[40] H. Theisel, J. Sahner, T. Weinkauf, H.-C. Hege, and H.-P. Seidel. Extraction of parallel vector surfaces in 3D time-dependent fields and application to vortex core line tracking. In *Proc. IEEE Visualization*, pages 631–638, 2005.

[41] H. Theisel and H.-P. Seidel. Feature flow fields. In *Proc. Symposium on Data Visualisation*, pages 141–148, 2003.

[42] Y. Tong, S. Lombeyda, A. N. Hirani, and M. Desbrun. Discrete multiscale vector field decomposition. *ACM Trans. Graph. (Proc. SIGGRAPH)*, 22(3):445–452, 2003.

[43] T. Weinkauf, J. Sahner, H. Theisel, and H.-C. Hege. Cores of swirling particle motion in unsteady flows. *IEEE Transactions on Visualization and Computer Graphics (Proc. Visualization)*, 13(6):1759–1766, 2007.

[44] T. Weinkauf and H. Theisel. Streak lines as tangent curves of a derived vector field. *IEEE Transactions on Visualization and Computer Graphics (Proc. Vis)*, 16(6):1225–1234, 2010.

[45] T. Weinkauf, H. Theisel, A. V. Gelder, and A. Pang. Stable feature flow fields. *IEEE Transactions on Visualization and Computer Graphics*, 17(6):770–780, 2011.

[46] J. Weiss. The dynamics of enstrophy transfer in two-dimensional hydrodynamics. *Physica D: Nonlinear Phenomena*, 48(23):273–294, 1991.

[47] A. Wiebel. Feature detection in vector fields using the Helmholtz-Hodge decomposition. Diploma thesis, Univ. Kaiserslautern, 2004.

[48] A. Wiebel, R. Chan, C. Wolf, A. Robitzki, A. Stevens, and G. Scheuermann. Topological flow structures in a mathematical model for rotation-mediated cell aggregation. In *Topological Methods in Data Analysis and Visualization*, Mathematics and Visualization, pages 193–204, 2009.

[49] A. Wiebel, C. Garth, and G. Scheuermann. Computation of localized flow for steady and unsteady vector fields and its applications. *IEEE Transactions on Visualization and Computer Graphics*, 13(4):641–651, 2007.